Geophys. J. Int. (2007) **168,** 1195–1209 doi: 10.1111/j.1365-246X.2006.03222.x

Limitations on the inversion for mantle viscosity from postglacial rebound

Archie Paulson, Shijie Zhong and John Wahr*

Department of Physics, University of Colorado, Boulder, CO 80309, *USA. E-mail: archie.paulson@colorado.edu*

Accepted 2006 September 8. Received 2006 September 7; in original form 2005 September 14

SUMMARY

Observations of postglacial rebound (PGR) can provide important constraints on mantle viscosity structure. In this study, we investigate how well PGR observations are able to constrain the spherically symmetric (1-D) viscosity structure of the Earth. We generate synthetic PGR data by calculating the response of an earth model with realistic 3-D viscosity. The viscosity model is constructed starting from seismic tomography models. We generate synthetic PGR data from this model including relative sea levels, exponential relaxation times, $\dot{J}_2$, polar wander, and GRACE time-variable gravity measurements, where most of the data is concentrated in the Laurentide region. We then attempt an inversion for a 1-D (spherically symmetric) viscosity structure based on minimizing the misfit to these PGR data. Using a Monte Carlo algorithm to invert for two layers of viscosity [upper and lower mantle (UM and LM)], we obtain well-constrained values which correspond to the two-layer average of the logarithm of the 3-D viscosity structure in the vicinity of Laurentia. We then attempt to invert for four layers of viscosity. In this case we find a 'trade-off effect' in which neighbouring layers may have highly variable viscosities while maintaining a constant average between them. Since the PGR data are insensitive to this trade-off in neighbouring layers, the viscosity of any one of the four layers cannot be well constrained. By repeating the inversion with synthetic data derived from an Earth model which itself is 1-D with four viscosity layers, we demonstrate that it is the insensitivity of the PGR data, not complications due to 3-D structure, that allow the trade-off effect and the resulting failure of the inversion. We also perform a resolution test to study the extent of the insensitivity of PGR to these viscosity trade-offs, finding that the limit of resolution in the UM is about the size of the entire UM, and similarly for the LM. This reinforces our findings that only two layers are obtainable in an inversion for viscosity from PGR.

Key words: glacial rebound, mantle viscosity.

1 INTRODUCTION

Mantle viscosity structure, playing an important role in our understanding of mantle dynamics, can be inferred from modelling long-wavelength non-hydrostatic geoid anomalies (Hager 1984; Richards & Hager 1984) and postglacial rebound (PGR) observations (Cathles 1975; Peltier 1976, 1998). While geoid modelling indicates that the lower mantle(LM) is significantly more ($\times 30$) viscous than the upper mantle (UM) (Hager & Richards 1989), some PGR modelling suggests a largely uniform mantle viscosity (e.g. Peltier 1998). However, other PGR modelling and the joint-modelling of PGR and geoid observations support the mantle viscosity structure derived from geoid studies (Lambeck 1995; Forte & Mitrovica 1996; Mitrovica 1996; Simons & Hager 1997).

In this study, we investigate the use of PGR as a tool for inferring mantle viscosity. Geological evidence, especially relative sea level (RSL) histories in regions of active surface adjustment, have long been available and used to this end (e.g. Tushingham & Peltier 1992). There have also been improvements in the measurement of global PGR signals, including $\dot{J}_2$ (Cox & Chao 2002; Cheng & Tapley 2004) and true polar wander (McCarthy & Luzum 1996), which have been exploited for their constraints on mantle viscosity structure. More recently, anticipation of large amounts of data from the GRACE mission, detailing secular time-variable gravity change, has raised hopes that these measurements may further improve the inference of viscosity structure (Velicogna & Wahr 2002).

With the data available, several attempts at inversion for mantle viscosity structure have been made. Mitrovica & Peltier (1995) and Peltier & Jiang (1996) used Bayesian inference procedures which

*Also at: Cooperative Institute for Research in Environmental Sciences, University of Colorado, Boulder, CO 80309, USA.

begin with a starting viscosity model and iteratively refine it to fit various PGR data sets. Kaufmann & Lambeck (2002) use a formal inverse procedure to infer a viscosity profile. These studies have arrived at many-layer viscosity models, implying a high-resolution understanding of the earth's 1-D viscosity structure. Similarly, Steffen & Kaufmann (2005) have performed an inversion from Fennoscandian PGR data that deduces a low-viscosity zone beneath the Barents Sea, though not beneath Scandinavia. While such models can undoubtedly reproduce well the observed PGR phenomena, some questions remain as to how well constrained these detailed models are and how 3-D mantle viscosity may influence the inverted 1-D structure. Kaufmann & Wu (2002) have used synthetic PGR data generated for Fennoscandia to find that an inversion for radial viscosity structure will return the local lithospheric thickness, but is complicated by lateral variations in athenospheric viscosity.

Aspects of the influence of 3-D mantle structure have been recently studied in, for example, Kaufmann *et al.* (2005), Wu & van der Wal (2003) and Latychev *et al.* (2005). Lateral variations in the lithosphere have also been shown to affect PGR observables (e.g. Martinec *et al.* 2001; Zhong *et al.* 2003). Paulson *et al.* (2005) have shown that the PGR of a 3-D Earth may be best reproduced with a 1-D viscosity model which reflects the viscosity structure beneath the glacial load. Although we see in these studies a measurable impact of 3-D structure on PGR, none of them has directly addressed the complications that lateral mantle heterogeneities may introduce in 1-D viscosity inferences.

In this paper, we wish to study how well PGR observations can constrain 1-D mantle viscosity models. Much of the work on mantle viscosity inference has sought a 1-D model to explain PGR data, and then interpreted the result as an average of the entire earth's viscosity; we wish to assess the accuracy of such an interpretation. We do so by first creating a realistic 3-D Earth proxy of known viscosity structure, computing its PGR response, then using these synthetic data in a Monte Carlo inversion to attempt to recover the correct viscosity. Unlike an inversion from actual PGR measurements, such a synthetic study allows us to evaluate the results of the inversion in terms of the known 'true' viscosity structure. We may ask, for example, what aspects of the true, complex viscosity structure appear in an inversion seeking the best two-layer viscosity model. Additionally, a Monte Carlo approach allows us to sample many very different viscosity models during the minimization of the misfit to PGR observations. Thus, rather than obtaining a single model of minimum misfit, we are able study the *ensemble* of viscosity models that sufficiently reproduce the synthetic data.

Evaluation of how well a particular viscosity model reproduces the synthetic PGR data is made more useful by considering the measurement uncertainties associated with the various types of data. Although the data themselves are produced synthetically, we use published values for uncertainties in these quantities. We may thus consider the ensemble of all models that reproduce the PGR within established measurement uncertainty, rather than simply minimizing the misfit. Variations in viscosity structure among the models of such an ensemble give information about how well constrained the various parameters are.

We begin with a general discussion of the procedures employed to solve for PGR deformation, and a description of the 3-D viscosity model we created for generation of the synthetic data. Section 3 then describes the results of attempts to invert for two or more layers of viscosity from the synthetic PGR data. Conclusions and discussion are given in Section 4.

2 CALCULATION OF THE PGR RESPONSE AND CONSTRUCTION OF A 3-D VISCOSITY MODEL

2.1 Model formulation and solution procedures

Calculation of PGR involves solution of the governing equations of mass and momentum conservation, along with gravitational perturbation via Poisson's equation (Wu & Peltier 1982). For our calculations we assume an incompressible Earth with self-gravitation, whose mantle is a Maxwell solid of uniform density overlying an inviscid core. The solution is obtained by solving the differential equations in the mantle, with effects of the core coming in through boundary conditions on the mantle solution. With the assumptions stated, the governing equations may be expressed as

$$u_{i,i} = 0, \tag{1}$$

$$\sigma_{ij,j} + \rho_0 \phi_{,i} - (\rho_0 g u_r)_{,i} = 0, \tag{2}$$

$$\phi_{,ii} = 0, \tag{3}$$

where the notation $A_{,i}$ represents differentiation of A with respect to coordinate x_i, u_i is the displacement, u_r its radial component, σ_{ij} is the stress tensor, ρ_0 is the unperturbed density, g is the magnitude of the gravitational acceleration, and ϕ is the perturbation of the gravitational potential. Note that the Eulerian density $\rho_1 = -(u_i\ \rho_0)_{,i}$ vanishes for the case of an incompressible mantle of uniform density (e.g. Zhong *et al.* 2003).

Boundary conditions are provided as follows. At the core–mantle boundary, $r = r_b$, continuity of normal stress above the fluid core provides that

$$\sigma_{ij} n_j = (\rho_c \phi - u_r \rho_c g) n_i \qquad \text{for} \qquad r = r_b, \tag{4}$$

where ρ_c is the constant core density and n_i is an outward-normal vector to the core–mantle boundary. At the surface, $r = r_s$, spatially and temporally varying glacial and ocean loads, discussed below, provide an applied pressure $\sigma_{\text{app}}(\theta, \varphi, t)$:

$$\sigma_{ij} n_j = -\sigma_{\text{app}}(\theta, \varphi, t) n_i \qquad \text{for} \qquad r = r_s, \tag{5}$$

where n_i is the surface normal. Finally, eq. (3) has boundary conditions given by

$$\phi(r^+) = \phi(r^-) \qquad \text{for } r = r_s \text{ and } r = r_b,$$

$$n_i \phi_{,i}(r^+) + 4\pi G \rho(r^+) n_i u_i(r) = n_i \phi_{,i}(r^-) + 4\pi G \rho(r^-) n_i u_i(r) \qquad \text{for } r = r_s \text{ and } r = r_b,$$

for a gravitational constant G, where $\rho(r^+) = 0$ at the outer surface.

With the equations above the stress tensor σ_{ij} and strain tensor ϵ_{ij} of a Maxwell incompressible solid are related by

$$\sigma_{ij} + \frac{\eta}{\mu}\dot{\sigma}_{ij} = -\left(P + \frac{\eta}{\mu}\dot{P}\right)\delta_{ij} + 2\eta\dot{\epsilon}_{ij}, \tag{6}$$

where η is the viscosity, μ is the shear modulus, P is the pressure, δ_{ij} is the Kronecker delta, and the dot indicates a time derivative. Other parameters used for this study are shown in Table 1. Shear modulus is constant throughout the mantle. The gravitational acceleration is also approximated by a constant throughout the mantle, but this is used only for calculations of the pressure provided by surface mass loads and does not imply a uniform gravitational potential.

The applied surface pressure, $\sigma_{\text{app}}(\theta, \varphi, t)$, is provided by changes in ice and ocean loads over the last glacial cycle. For the ice load, we

Table 1. Model parameters.

Parameter	Value
Radius of Earth, r_s	6.3700×10^6 m
Radius of CMB, r_b	3.5035×10^6 m
Mantle shear modulus, μ	1.4305×10^{11} Pa
Mantle density, ρ_o	4400 kg m^{-3}
Density change across CMB, $\Delta\rho$	5425 kg m^{-3}
Gravitational acceleration, g	9.8 m s^{-2}

use the ICE-3G deglaciation model (Tushingham & Peltier 1991) which specifies global ice height at 1 kyr intervals over the last 14 kyr. We linearly interpolate between these times and provide a 90 kyr linear ramp up to glacial maximum. The ocean load at any given place and time, $L_o(\theta, \varphi, t)$, is determined by the PGR-induced perturbations to the geoid and surface displacement (N and U, respectively) via the sea level equation (Farrell & Clark 1976):

$$L_o(\theta, \varphi, t) = [N(\theta, \varphi, t) - U(\theta, \varphi, t) + c(t)]O(\theta, \varphi, t), \tag{7}$$

where $O(\theta, \varphi, t)$ is the time-dependent ocean function (1 over ocean, 0 elsewhere) and c is the eustatic sea level change, given by

$$c(t) = \frac{1}{A_o(t)}\left[-\frac{M_{ice}(t)}{\rho_w} - \int (N - U)O \, d\Omega\right], \tag{8}$$

where A_o is the area of the oceans, M_{ice} is the mass of the ice sheets, ρ_w is water density, and $d\Omega$ is an element of solid angle.

Calculation of the PGR response also includes the feedback due to polar wander: perturbations to the Earth's inertia tensor (by changes in surface deformation and loading) alter the rotation vector, which perturbs the centrifugal potential, which in turn affects the deformation (Wu & Peltier 1984). We use the improved formulation of polar wander feedback described in Mitrovica *et al.* (2005) and Paulson *et al.* (2005), in which the Earth's initial background oblateness is computed without elastic lithospheric stress, and is amplified slightly (about 0.8 per cent) to accommodate the Earth's observed excess ellipticity. These two corrections, discussed in detail in Mitrovica *et al.* (2005), serve to stabilize and reduce the response of the rotation axis to deformation and surface load changes.

For this study, the theoretical formulation discussed above is implemented with two separate solution procedures: a spherical finite element code that can accommodate a realistic 3-D viscosity model, and a faster spectral code for simpler 1-D viscosity models. The finite element code CitcomSVE, discussed in detail in Zhong *et al.* (2003) and Paulson *et al.* (2005), is used to generate synthetic data from earth models with 3-D viscosity. The spectral method is similar to that of Wu & Peltier (1982) and Wahr *et al.* (2001)—it computes deformation via Love numbers in the Laplace transform domain using the collocation technique (Mitrovica & Peltier 1992). The spectral method is used to run fast forward models for the Monte Carlo inversion. Greater detail on these two methods, benchmarks between them, and implementation of the ocean loading and polar wander feedback are given in Paulson *et al.* (2005).

2.2 3-D viscosity model

To make the inversion as realistic as possible, we create an earth model with plausible viscosity structure for generation of the synthetic PGR data. This is accomplished by conversion of shear wave velocity models into a global 3-D temperature field, which is then converted to viscosity. The method is discussed here, with greater detail provided in Paulson *et al.* (2005).

We begin with a composite of two shear wave velocity models: the long-wavelength global model S20RTS (Ritsema *et al.* 1999), and the higher resolution model NA00 of van der Lee (2002) beneath North America (the latter is included because much of our work centres on Laurentia). The provided shear velocities are converted to a 3-D temperature structure. This is accomplished by direct conversion based on mineral properties (Shapiro & Ritzwoller 2004) for depths less than 400 km. At greater depths, a constant conversion to density variation is used ($\delta\ln\rho/\delta\ln V_s = 0.3$, Karato (1993)), the resulting density variation is then multiplied by a depth-dependent thermal expansivity to obtain 3-D temperature variations $\delta T(\mathbf{r})$, which are added to the adiabatic temperature gradient to obtain a global 3-D temperature field, $T(\mathbf{r})$. (Note, $\mathbf{r}$ indicates a 3-D function of position.) The 3-D viscosity $\eta(\mathbf{r})$ is then computed with

$$\eta(\mathbf{r}) = A_o \exp\left[\gamma \frac{T_m(r)}{T(\mathbf{r})}\right], \tag{9}$$

where $T_m(r)$ is the melting temperature, γ is an activation parameter, and A_o is a coefficient (Yamazaki & Karato (2001) as used in McNamara *et al.* (2003)). We may choose γ and the leading constant A_o separately for the UM and LM to obtain a desired viscosity discontinuity at 670 km depth (for example, a jump by a factor of 30, or a factor of 2). The model's lithospheric (elastic) thickness is derived separately, using gravity and topography from sea-mounts in oceanic regions and from long-term loads and heat-flux in continental regions (Zhong *et al.* 2003). The lithospheric thickness used reflects that of PGR timescales, and is given in the symbol T_e for in this study. The resulting lithosphere varies in thickness from a prescribed minimum of 20 km (near plate boundaries) to a maximum of about 230 km (in the continental root of North America).

For this study, we have chosen a value of $A_o = 2 \times 10^9$ Pa s in the UM and $A_o = 1.2 \times 10^{13}$ Pa s in the LM, giving a viscosity discontinuity of 30× at a depth of 670 km. Fig. 1(a) shows the resulting vertical structure, with the global average represented by the black line, and the extent of the lateral variations shown in grey (more figures of the viscosity model are available in Paulson *et al.* 2005). Lateral variations at a given depth typically vary by about two to three orders of magnitude.

We do not claim that this procedure provides a definitive viscosity model of the Earth. However, we consider this model to be a reasonable proxy for the Earth to generate synthetic PGR data, as we will do in Sections 3.2 and 3.3. This model exhibits viscosity variations similar to those described in Ivins & C (1995).

2.3 PGR observations

Postglacial rebound is observable in several geophysical measurements: RSL change, the secular trend of J_2, true polar wander, and is expected to be observable in GRACE time-variable gravity data. For this study, we generate synthetic PGR data to investigate the effectiveness of inversion for viscosity. Thus, in all cases our synthetic data enjoy the somewhat unrealistic advantage that the entire signal is due exclusively to the glacial isostatic adjustment to the loads that we impose. For example, though it has been suggested that the current secular rate of change of J_2 may be partially due to present-day changes in Greenland and Antarctic ice sheets, changes in J_2 in our synthetic data can only result from PGR. This simplification may be interpreted as the assumption that for all data used in a viscosity inversion, one is able to extract the component which is due to PGR. Although this may seem an overly optimistic assumption, we will find (Section 4) that it does not alter our basic conclusions.

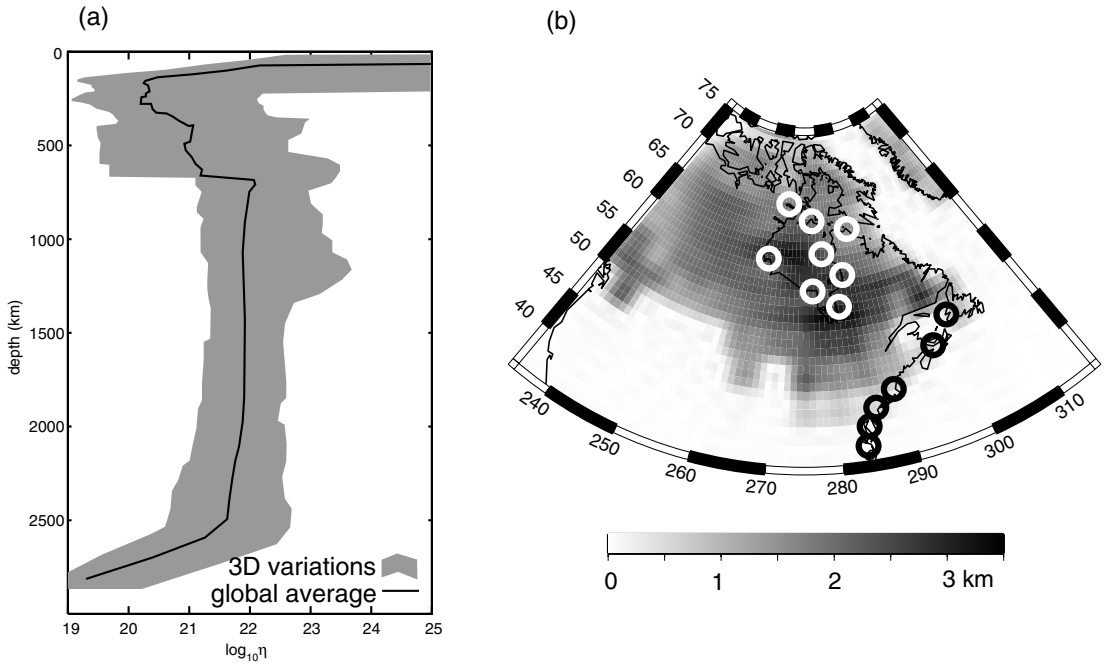

Figure 1. (a) A view of the 3-D viscosity model derived from seismic tomography. The lateral variations are shown in grey; the line shows the 1-D global average of the logarithm of the viscosity. (b) The ICE-3G model at glacial maximum with the site of RSL measurements. White circles are the Hudson Bay sites (used for calculation of relaxation times), and black circles are the east coast sites.

Although the data are derived synthetically, we use uncertainties from published measurement errors, as discussed below. Using synthetic data with true measurement error bars will allow us to identify those 1-D viscosity models which provide PGR measurements sufficiently close to the synthetic data.

The PGR observations we use for the synthetic data are described here. Some examples derived from the 3-D calculation are shown in Fig. 2 and discussed below. The viscosity models that are used to generate the synthetic data for the inversions below are

(1) the 3-D viscosity model derived in the previous section (used in Sections 3.2 and 3.3),
(2) a four-viscosity-layer model (in Section 3.4) and
(3) a uniform viscosity model (in Section 3.5)—the layered viscosity models are discussed further in those sections.

For six sites along the east coast of North America, shown in Fig. 1(b) (black circles), our 3-D model provides relative sea level (RSL) at several times over the last few thousand years. For our purposes, RSL is defined as the geoid change (representing the ocean's surface) minus the topography change due to deformation, with respect to the present-day values. The synthetic data along with uncertainties and measurement times for a sample site, Cape Charles, Virginia, are shown in Fig. 2(a). We use the RSL database (Tushingham & Peltier 1992) which provides RSL histories and uncertainties at 392 sites globally extending up to 14 kyr before present to determine the measurement times and uncertainties for our synthetic data. This allows us to simulate the amount of PGR information available for an inversion from true (as opposed to synthetic) data. Thus, the times of measurement (extending, for example, back to 15 kyr BP for the site shown in Fig. 2a) are those provided in the Tushingham & Peliter RSL database, and the errorbars are the same as those in the database (altered slightly as described presently).

The uncertainty in the time of an RSL measurement (the horizontal error bars in Fig. 2a) is slightly complicating, since production of the synthetic data as well as the recording of data from any 1-D forward model in the Monte Carlo inversion procedure (discussed later) requires precise times at which to record the RSL for a given site. That is, since this is a purely synthetic study we must specify *exactly* at which times we record our RSL values, leaving no time-uncertainty in the synthetic data; however, since we would like to use errorbars on these data that reflect the uncertainty in actual, available data, we must somehow accommodate the fact that there is uncertainty in both the sea level height and the time of measurement. This time-uncertainty slightly increases the spread in data which can be considered to fit the data. We accommodate this slight increase by recording the RSL at the 'best' times (at the centre of each error bar) given in the RSL Database, and then amplifying the RSL uncertainty by an amount that reflects the corresponding uncertainty in its time of record. Specifically, the RSL error (σ_{RSL}), the time error (σ_t) and θ, the angle formed by the line between a data point and its neighbour (relative to horizontal) are combined to form the new error for the RSL at that time: $\sigma = \sigma_{\mathrm{RSL}}\sqrt{1 + (\sigma_t \tan\theta/\sigma_{\mathrm{RSL}})^2}$. The resulting uncertainties are typically 12 per cent larger than the original σ_{RSL}.

A similar procedure is used to generate synthetic RSL measurements at eight sites around Hudson Bay (white circles in Fig. 1b). At each site, the measurement can be closely approximated with a single, exponentially decaying function of the form $a[\exp(-t/\tau) - 1]$. Note that this is only an approximation due to the multiple modes of relaxation and to ongoing load changes from changing sea levels, but the approximation appears to be robust (Mitrovica & Peltier 1995). For real data it is usual to determine the best-fitting 'relaxation time' τ at each site, and to use τ to constrain PGR. This reduces the dependence of the constraint on the ice model. We adopt this same procedure for our synthetic data, fitting only back as far as

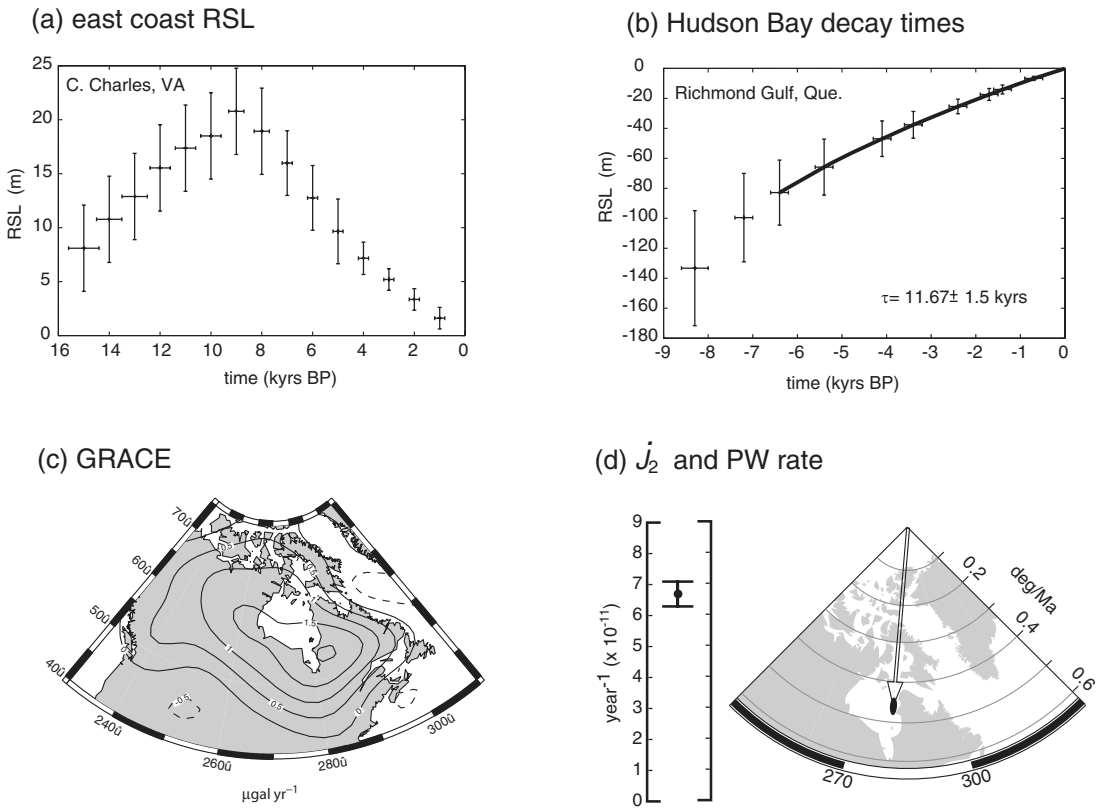

Figure 2. Synthetic PGR data used in this study. The data values shown are derived from the 3-D viscosity model. (a) Relative Sea Level (RSL) at Cape Charles, VA, shown with errorbars. (b) RSL at Richmond Gulf, Quebec, along with the exponential fit, resulting in a relaxation time of 11.67 ± 1.5 kyr. (c) Secular change in gravity field around Hudson Bay (simulated GRACE data), in m s^{-2} per year. (d) $\dot{J}_2$ and polar wander rate.

6 kyr BP so as not to include times when glacial ice remained in Laurentia. Although we do not demonstrate it here, we find that use of the raw RSL data (as done with the east coast sites) provides a similar constraint on the inversion as does use of the relaxation times alone. Uncertainty in the relaxation time for each site is also derived from the RSL Database by taking the one standard deviation spread in relaxation times in a large random sample of a and τ, whose exponential forms fit within one χ^2 of the RSL curve, using the errorbars provided in the RSL Database. A sample site, at Richmond Gulf, Quebec, is shown in Fig. 2(b), showing the synthetic RSL data and the exponential fit to it.

Looking ahead, we anticipate the GRACE mission to provide a significant amount of information relevant to PGR in the form of the secular change in higher order gravity Stokes coefficients. Use of this information also requires anticipation of the contamination of the secular signal by present-day ice mass changes in Antarctica and Greenland as well as by other signals around the globe that could appear to be secular when averaged over the nominal 5-yr lifetime of GRACE (Velicogna & Wahr 2002). Such a signal contamination may be largely avoided by considering the Stokes coefficients summed into a gravity field in only the Laurentide region, where the secular change is expected to be dominated by PGR. We use this approach in the current study, including spherical harmonic degrees up to 30. Uncertainties on the secular trend in the GRACE data are taken from a generalization of the technique used by Wahr *et al.* (2004), supposing 5 yr of data collection. This involves taking the 'calibrated errors' in the Stokes coefficients provided by the GRACE project, δC^i_{lm} and δS^i_{lm} (where i indicates the month, up to N) and computing the RMS gravity error $\sigma(\theta, \varphi)$ by

$$\sigma(\theta,\varphi) = \sqrt{\sum_{l,m}\left(F^2_{lm}\left[\sum_{i=1}^{N}\frac{(\delta C^i_{lm})^2}{N}\right] + G^2_{lm}\left[\sum_{i=1}^{N}\frac{\left(\delta S^i_{lm}\right)^2}{N}\right]\right)}, \tag{10}$$

where the F_{lm} and G_{lm} are the functions (proportional to the spherical harmonic functions) that provide the spatial gravity field $g(\theta, \varphi)$ from the Stokes coefficients via

$$g(\theta,\varphi) = \sum_{l,m}\left[F_{lm}C_{lm} + G_{lm}S_{lm}\right]. \tag{11}$$

Finally, the error in the secular signal can be reduced by fitting the secular trend to the N months of data (in this case, $N = 60$ months); this reduction is given by

$$\sigma \rightarrow 12\sigma\sqrt{12/\left[(N-1)\,N\,(N+1)\right]} \tag{12}$$

(Wahr *et al.* 2000). The resulting spatial error field is a uniform increase in error with decreasing latitude.

The GRACE data (in the form of secular Stokes coefficients to a gravity field) are summed to produce the gravity field. This has the advantage of slightly emphasizing the shorter wavelengths (compared to the geoid) with a factor of $(l + 1)$. The reason for using a gravity sum rather than geoid is twofold: to exploit the shorter-wavelength information which would be small compared to the long-wavelength geoid signal, and to prevent some of the long-wavelength leakage from the nearby mass change in the Greenland ice sheets. The resulting (synthetic) secular rate of change of gravity in the region of interest is shown in Fig. 2(c).

To compare the GRACE data between models, the computed gravity rate is summed onto a grid of 120 points, distributed for equal area per point, within the 1.5 μgal yr^{-1} contour in Fig. 2(c). Misfit to the GRACE data is then computed with

$$\chi^2_{\mathrm{GRACE}} = \frac{1}{M}\sum_{j=1}^{M}\left(\frac{g_j^{\mathrm{data}} - g_j^{\mathrm{model}}}{\sigma_j}\right)^2, \quad (13)$$

where $M = 120$ and the σ_j are from eq. (12). Since the model gravity fields are relatively smooth (Fig. 2c) their average χ^2 is fairly independent of M, the number of points used in the summed field.

Finally, we consider two long-wavelength signatures of PGR: $\dot{J}_2$ and the rate of polar wander. The error bars on both are taken from just the measurement uncertainty, thus we implicitly assume that we are considering only the PGR component of these quantities. The secular rate of J_2 has been estimated to be 2.75×10^{-11} yr^{-1} by Cox & Chao (2002) and to be 1.96×10^{-11} yr^{-1} by Cheng & Tapley (2004). We take half the difference between these two estimates for the uncertainty on this datum (Fig. 2d). Uncertainty for the polar wander rate is obtained from McCarthy & Luzum (1996), who give the present day rate to be 0.925 ± 0.022 degrees Myr^{-1} in the direction of 75.0 ± 1.1 degrees West. As before, we take the uncertainties from these measurements and put them on our synthetically generated data. The results for the 3-D viscosity model are shown in Fig. 2(d), where the polar wander uncertainty is shown as the small black ellipse. Note that the observed values quoted here are not shown in Fig. 2 (the values shown are the generated synthetic data), but the errorbars on those values are taken from the published data.

3 MONTE CARLO INVERSION

3.1 Method

The inversion for viscosity is accomplished by a Monte Carlo method employing a χ^2 (chi-squared) measure of misfit and a simulated annealing method of parameter search (Sambridge 1999; Agostinetti *et al.* 2004). As mentioned, the synthetic PGR data (RSLs, GRACE gravity field, $\dot{J}_2$, and polar wander rate) are generated from the 'true' earth model. The term 'true' viscosity, for purposes of this study, refers to the viscosity model which provides the synthetic data; in most cases it is the model with the 3-D viscosity derived in Section 2.2 and run with the spherical finite element method (Zhong *et al.* 2003; Paulson *et al.* 2005). The goal is to reconstruct as much of the 'true' viscosity as possible using only PGR data. To do this, we run an ensemble of forward models with 1-D viscosity structures (for example, models with two layers of viscosity) using the spectral method (Wu & Peltier 1984; Wahr *et al.* 2001; Paulson *et al.* 2005), then record the resulting PGR observables and compare them to the synthetic data.

For comparison of the results of a given 1-D forward run to the synthetic data we require a single measure of misfit to all the PGR data discussed in Section 2.3. Knowing the uncertainties (σ_i) in the synthetic data it is natural to use a χ^2 measure of misfit:

$$\text{misfit} = \chi^2 = \frac{1}{n}\sum_{i=1}^{n} w_i\left(\frac{m_i - s_i}{\sigma_i}\right)^2, \quad (14)$$

where the m_i are the PGR measurements for a given forward model, s_i are the corresponding synthetic data, w_i are relative weights (with $\sum_i w_i = 1$), and n is the total number of measured values. Note that every recorded number (e.g. every RSL at every time for the east coast data) is considered one of the m_i. Although not presented here, we experimented with a variety of weighting schemes and found little change to our conclusions (presented below). For the present study, we choose the weights w_i such that the following are true:

(a) the east coast RSL data, the Hudson Bay relaxation time data, the GRACE data, and the combined $\dot{J}_2$ and polar wander rate each share one quarter weight in the total misfit;
(b) all east coast RSL sites have equal weights;
(c) all Hudson Bay relaxation times have equal weights;
(d) GRACE data have a uniform weight per area
(e) the magnitude of $\dot{J}_2$, the direction of polar wander, and the magnitude of the polar wander rate are all equally weighted.

With such a misfit measure, we may judge whether a set of PGR observations is generally within measurement uncertainty of the synthetic data ($\chi^2 < 1$) or lies mostly outside the errorbars ($\chi^2 > 1$).

The inversion involves running thousands of forward models, searching for those which minimize misfit to the PGR data. All forward runs have the same ice model as used for the generation of synthetic data (ICE-3G as described in Section 2.1). For a two-layer inversion, we choose a lithospheric thickness and allow two layers of the mantle to vary their viscosity independently. In this case, the parameter space one must search through is only 2-D and so we perform a straightforward gridsearch of all reasonable parameter values. For more than two layers of viscosity, the increased dimensionality requires a Monte Carlo approach to sample the parameter space—we employ a simulated annealing algorithm enhanced by the neighbourhood algorithm (Sambridge 1999). This method samples the parameter space randomly at first, and then concentrates the sampling closer to the models of lower misfit. The rate at which the algorithm converges to a particular neighbourhood of parameter space can be slowed to allow a very broad sampling of parameter space. As we find in Section 3.3, a broad sampling of models where $\chi^2 < 1$ is important to identify those well-fit models which are far away in parameter space from the single best-fitting model. Although searching only in the near vicinity of the current best-fitting model will find a model of small misfit, this tends to miss regions of parameter space which also have misfits of $\chi^2 < 1$. We will be interested not so much in the model of minimum misfit as in the entire ensemble of models that can be considered to fit the data.

3.2 two-layer inversion from 3-D Earth

With the synthetic PGR data derived from the 3-D viscosity model, as discussed above, we first search for the two-layer viscosity model that best reproduces that data. The two layers represent the UM and LM, divided at 670 km depth. The depth of the division was chosen to correspond to the discontinuity known to exist in the 3-D model (seen in Fig. 1a). We perform a two-parameter gridsearch, running models at all viscosity combinations in uniform steps of 0.05 in base-10 logarithm of viscosity in Pa s.

To set the elastic lithospheric thickness for the two-layer models, a preliminary inversion run was performed with three parameters: UM viscosity, LM viscosity and T_e, the elastic lithospheric thickness. The T_e of best fit was determined to be 150 km (this is approximately the elastic thickness in the vicinity of Laurentia in the 3-D model). We use $T_e = 150$ km for the two-layer gridsearch runs.

Results of the gridsearch are shown in Fig. 3(a), showing the χ^2 misfit of the two-layer models to the 3-D model results (i.e. the

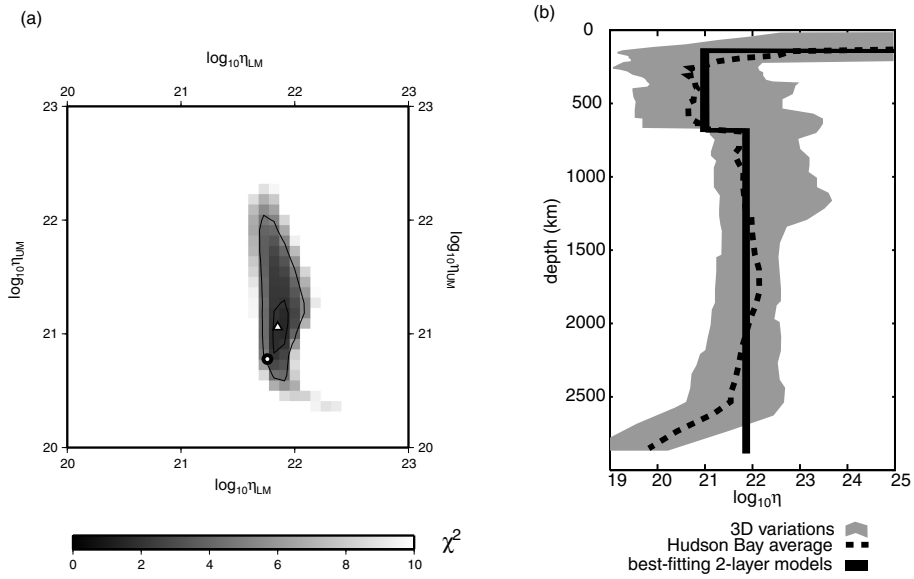

Figure 3. (a) The χ^2 misfit of the two-layer models run in a gridsearch, with UM viscosity on the vertical axis and LM viscosity on the horizontal axis. Contour lines are shown at $\chi^2 = 2$ and 5. The triangle indicates the two-layer average of the 3-D model in the vicinity of Hudson Bay—it also corresponds to the point of smallest misfit, at $\chi^2 = 1.45$. The circle shows the global two-layer average. (b) The ensemble of best-fitting two-layer models (i.e. those with $\chi^2 < 1.5$), shown in the black region. Also shown are the lateral variations in the 3-D viscosity model (grey) and the 1-D average of the viscosity in the Hudson Bay region (dashed line). The models shown are taken from those run in the gridsearch (Fig. 3), along with additional runs from the Monte Carlo algorithm. A large number of models, those with $\chi^2 > 1.5$, are not shown on the plot.

synthetic data). The figure shows the models with layer viscosities between 10^{20} and 10^{23} Pa s, with contours at $\chi^2 = 2$ and 5. The inversion clearly favours particular values for the UM and LM viscosities: $\eta_{\rm UM} = 1.00 \times 10^{21}$ Pa s and $\eta_{\rm LM} = 7.08 \times 10^{21}$ Pa s. However, as seen from the lowest χ^2 misfit at 1.45, even this best two-layer model cannot fit all the PGR data to within the data uncertainties.

The PGR observations for the lowest misfit model are shown in Fig. 4, along with its itemized (per observation) χ^2 misfits. The east coast RSL data are fit quite well ($\chi^2 = 0.25$ average for all sites). Fig. 4(a) shows the site at Cape Charles, Virginia, which lies nearly at the 1σ level. The eight relaxation times together give $\chi^2 = 1.08$ (the site at Richmond Gulf is shown in Fig. 4b). The GRACE data are shown as a map of the χ^2 values in Fig. 4(c); they average to $\chi^2 = 2.36$. $\dot{J}_2$ lies within the error bars: $\chi^2 = 0.36$ (Fig. 4d). The true polar wander rate falls outside the error ellipse by more than 1σ: $\chi^2 = 2.36$ (Fig. 4d).

For a synthetic study such as this, we know the 'true' viscosity of the Earth and can investigate how the best two-layer model compares to it. We find that the viscosity model of lowest misfit corresponds well to an average over the Laurentide region into two layers of the logarithm of the 'true' 3-D viscosity. This average model is shown with the triangle in Fig. 3(a)—it has viscosities $\eta_{\rm UM} = 1.10 \times 10^{21}$ Pa s and $\eta_{\rm LM} = 7.09 \times 10^{21}$ Pa s. Note that a *direct* averaging of local viscosity (i.e. averaging the viscosities, not their logarithm) would provide very different values, $\eta_{\rm UM} = 6.8 \times 10^{21}$ Pa s and $\eta_{\rm LM} = 9.3 \times 10^{21}$ Pa s, and yield a much larger misfit at $\chi^2 = 7.43$. We conclude from this that inversion for viscosity from PGR data will recover the log-average of the Earth's viscosity. Furthermore, the log-average recovered by the two-layer inversion is that of the *local* viscosity structure—this means only the viscosities beneath Hudson Bay are averaged together (in particular, beneath Hudson Bay and the regions within 100 km of its coastline). For comparison, a global log-average yields $\eta_{\rm UM} = 6.02 \times 10^{20}$ Pa s and $\eta_{\rm LM} = 5.75 \times 10^{21}$ Pa s; this viscosity and the resulting misfit are shown in Fig. 3(a) with a circle. The two-layer inversion, then, yields the *local* viscosity structure rather than a global average (the triangle and circle in Fig. 3(a), respectively). The ensemble of two-layer models with $\chi^2 < 1.5$ are shown in Fig. 3(b), together with the extent of the lateral viscosity variations of the 'true' Earth (grey).

Another way to visualize the inversion results is with Fig. 5(a). Here, for every forward run in the inversion, we place a point marking its χ^2 misfit on the horizontal axis, and on the vertical axis a measure of the average viscosity difference between that two-layer model and the true 3-D viscosity. The average viscosity difference is computed by differencing the logarithm of the viscosities of the two models, then averaging (as rms) those differences in the region beneath Hudson Bay (the same region as that described in the previous paragraph). This difference (Δ) may be expressed as

$$\Delta = \langle \log_{10} \eta_{\rm 3D}(r, \theta, \varphi) - \log_{10} \eta_{\rm 2L}(r) \rangle_{\rm HB} \qquad (15)$$

where $\langle \ldots \rangle_{\rm HB}$ indicates a rms average over Hudson Bay (and within 100 km of its coastline), $\eta_{\rm 3D}$ is the 'true' 3-D viscosity and $\eta_{\rm 2L}$ is a two-layer model. The average is performed over lateral and vertical dimensions, where the latter has is weighted by r^2 . Δ will thus have units of $\log_{10}$(Pa s), with smaller values representing better recovery of the true local viscosity structure. The dashed horizontal line in the figure represents the smallest viscosity difference possible for a two-layer model. The fact that the lowest misfit runs also have the best viscosity recovery demonstrates that the inversion is working: as the inversion works its way towards the left on this diagram, minimizing the misfit, it will also be approaching the actual two-layer average of the viscosity beneath Hudson Bay (the inversion has no knowledge of the viscosity recovery, the vertical axis, only the misfit to PGR data). The narrow tail on the left edge of the cluster of points is also significant, indicating that *all* models of small PGR misfit have similar viscosity structure; the viscosities returned by the inversion are well-constrained. Though this may be as expected, the

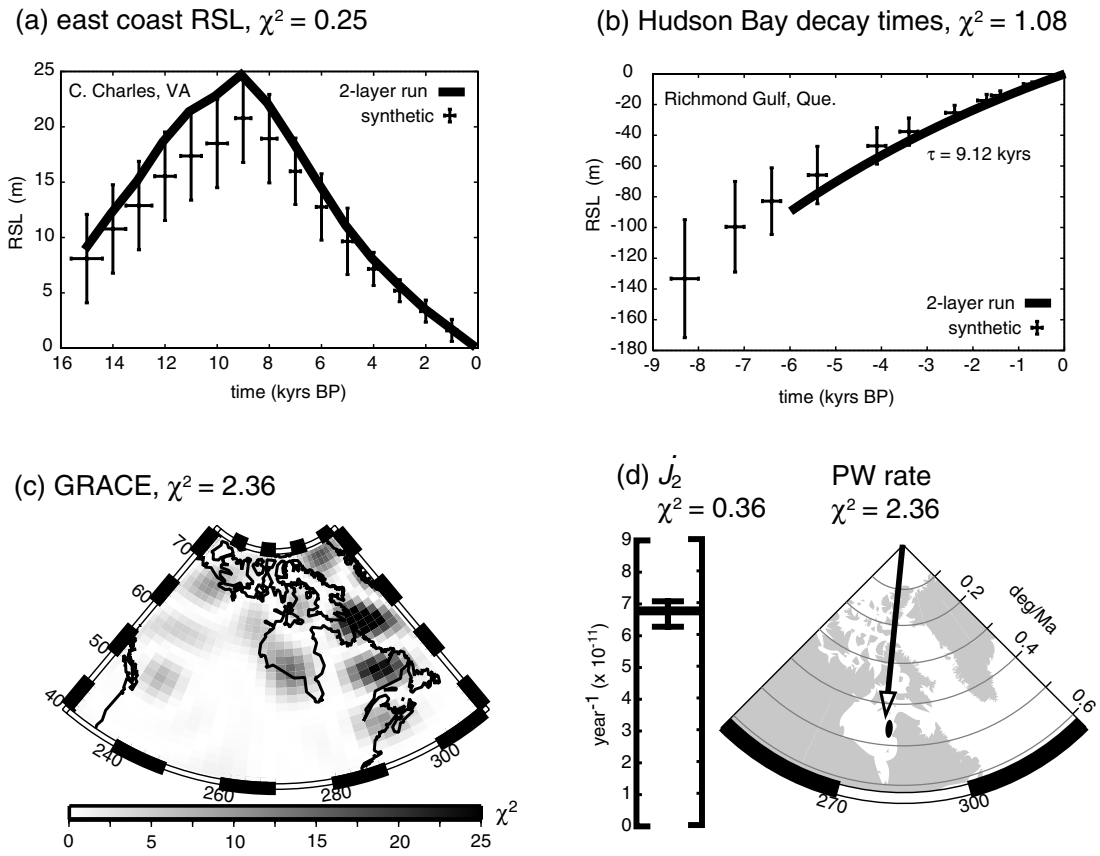

Figure 4. The PGR observations (Fig. 2) for the best-fitting two-layer model. (a) RSL at Cape Charles, VA. The errorbars show the synthetic data and the solid line is from the two-layer run. The average misfit for all east coast RSL sites is $\chi^2 = 0.25$. (b) Exponential fit to RSL at Richmond Gulf, Quebec. Average misfit for all sites is $\chi^2 = 1.08$. (c) A map of the χ^2 values for misfit to the GRACE gravity data; average is $\chi^2 = 2.36$. (d) $\dot{J}_2$ and polar wander rate with misfits of $\chi^2 = 0.36$ and 2.36, respectively.

conclusion will not hold in the following sections when we attempt to invert for a greater number of viscosity layers.

With a similar plot we may demonstrate the influence of performing an inversion with uncertainty in the glaciation model. For this purpose, we use the same synthetic PGR data described above (Section 2.3), but run the 1-D models in the inversion with the ICE-4G deglaciation model (Peltier 1994). The latter model differs from ICE-3G by having about 20 per cent more ice over Hudson Bay at glacial maximum and deglaciating with a slightly different spatial dependence; both ice models have zero ice mass change in North America after 4 kyr before present. The resulting plot of misfit versus viscosity difference (Δ) is shown in Fig. 5(b). The misfits are now much greater, due largely to the greater mass of ice used in the inversion runs. However, the fact that the models of lowest misfit also have the smallest difference with respect to the local two-layer log-average of the 3-D structure (i.e. the lowest values of Δ) shows that the preferred two-layer structure is the same as that from the previous inversion. Thus uncertainties of this sort in the ice model, though they may increase the misfit to PGR data, may not hinder the inversion's ability to find the correct two-layer structure.

3.3 Four-layer inversion from 3-D Earth

We next seek a greater amount of information from the inversion, attempting to invert for four layers of mantle viscosity. The four layers are those obtained by simply dividing in half each of the two layers considered above. The elastic lithospheric thickness, T_e, is again set to 150 km. The inversion proceeds by a simulated annealing algorithm which samples the 4-D parameter space in search of the model of lowest misfit to the synthetic PGR data. We are careful not to allow the sampling algorithm to focus in on one region of the parameter space too rapidly, so that samples are still spread broadly in parameter space in search of other misfit minima.

Since we cannot visualize the 4-D parameter space, we present the inversion results in the form of the scatter plot discussed for the two-layer case (Fig. 6a): each four-layer model has a point at its average difference from the true viscosity (Δ, vertical axis) versus its misfit value (χ^2, horizontal axis). The results are dramatically different from the two-layer inversion. The most obvious change is that the lowest misfit models (on the left edge) now have a large range of average viscosity difference with respect to the true 3-D viscosity. Although the lowest misfit, $\chi^2 = 0.61$, is now significantly lower than the best two-layer model misfit, there are a large number of four-layer models that fit the synthetic PGR data nearly equally well but with substantially different viscosity structures. If one considers all the four-layer models that fit the PGR data to within measurement uncertainty (roughly $\chi^2 \leq 1$), one finds models near the top of the diagram that may differ from the 3-D viscosity structure by nearly one order of magnitude on average (i.e. a log-average viscosity difference near one). Again, the dashed line near the bottom of Fig. 6(a) represents the best possible viscosity recovery by a four-layer model of the 3-D structure (naturally less than that for two-layer models).

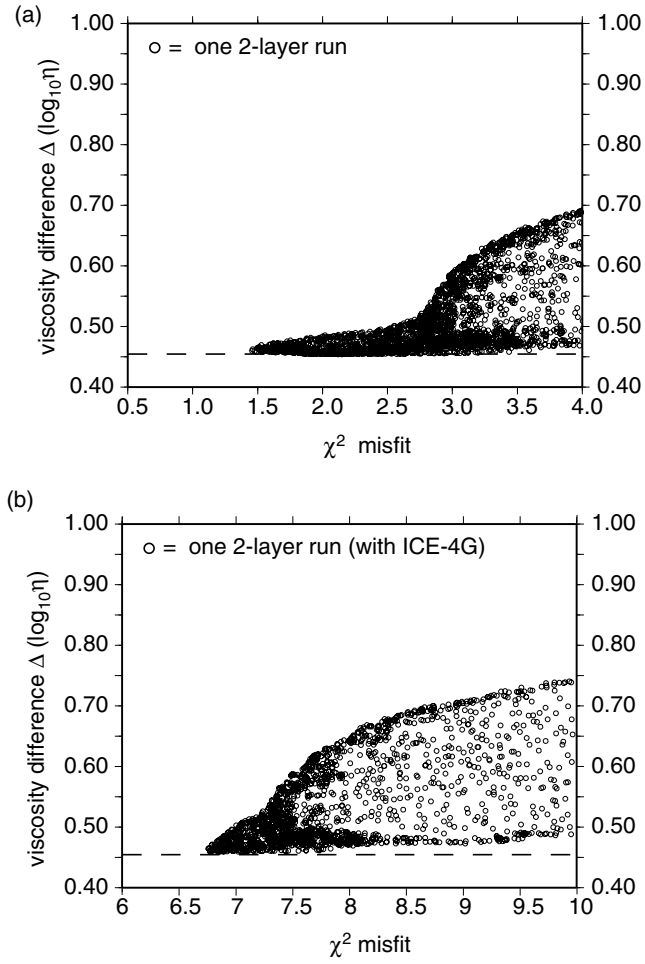

Figure 5. (a) A plot of some of the two-layer runs, placing a circle at each model's viscosity difference (with respect to the 3-D viscosity), Δ, versus its χ^2 misfit. The value Δ is computed with eq. (15). The dashed line near the bottom of the plot indicates the smallest possible viscosity difference between a two-layer model and the 3-D structure. The narrow tail at low misfit indicates that the inversion produces well-constrained values of viscosity. (b) A new two-layer inversion testing the effects of uncertainty in the glaciation model. The synthetic data are generated using ICE-3G, while the inversion models were run with ICE-4G. The two-layer local log-average of the 3-D viscosity is again the best-fitting model; this is demonstrated by the fact that the models of lowest misfit are also of lowest difference with the 'true' model. The misfits are much higher than in the previous inversion, due largely to the ∼20 per cent larger ice mass in ICE-4G.

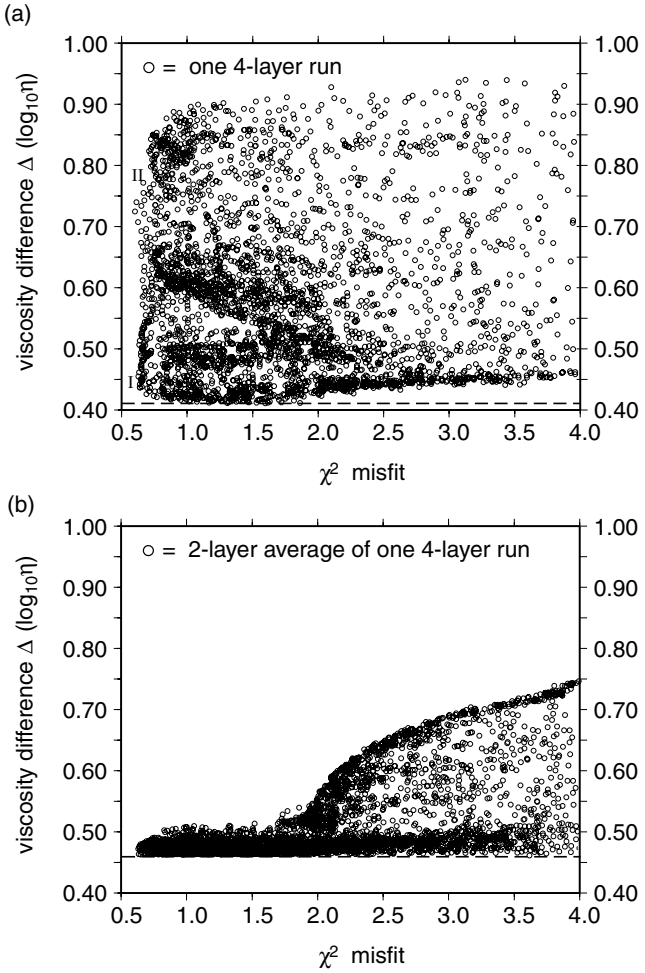

Figure 6. (a) The four-layer runs of lower misfit, placing a circle at each model's viscosity difference with respect to the 3-D viscosity, Δ, versus its χ^2 misfit. Only the models with $\chi^2 < 4$ are shown. The dashed line indicates the smallest possible Δ for a four-layer model. For this inversion there are many different models with a viscosity difference as high as 0.9 that fit the PGR data to within $\chi^2 < 1$, indicating highly variable viscosity values. Two models of low misfit (I and II) are marked in the plot, the former with good viscosity recovery and the latter with poor viscosity recovery. (b) When the four-layer viscosity models (from Fig. 6a) are averaged into two-layer models, the viscosity difference (Δ) values are replotted as shown here. Misfit values are unchanged. The inversion is now much better constrained, indicating that the trade-off effect was responsible for the poor constraints of the four-layer inversion.

The wide variety of models with low misfit suggests that an inversion with a smaller focus in parameter space may arrive at any of the models near the left edge, failing to detect the other models of significantly different viscosity structure that may also yield a low misfit. This could be the case, for example, for a simulated annealing algorithm with faster 'cooling', or by incrementally tweaking a starting model in directions that lower the misfit.

To understand Fig. 6(a) better, we select two models near the left edge, but at different ends of the vertical scale, labeled 'I' and 'II' in the figure. These two viscosity models are shown in Fig. 7. It is evident that model I ($\chi^2 = 0.61$) has a good viscosity recovery, while model II ($\chi^2 = 0.67$) has a poor viscosity recovery (small and large values of Δ, respectively). However the two models differ in a systematic way: compared to model I, model II appears to have compensated for a lower viscosity in the uppermost layer with a correspondingly higher viscosity in the adjacent layer, and a similar trade-off appears in the two LM layers. Further investigation of the low misfit models demonstrate that this relationship is not coincidental, but is the primary source of the large variability in viscosity structures among well-fitting models. It should be noted here that, although Fig. 6(a) appears densely populated, this does not imply that *any* four-layer viscosity model with an average viscosity difference up to 0.9 will fit the PGR data well, but that there are many different models that can. In fact these well-fitting models are related in a systematic way, involving viscosity trade-offs in neighbouring layers, as discussed below. Future studies are needed to examine whether this type of trade-off can be removed with additional constraints such as the long-wavelength geoid (Hager & Richards 1989; Mitrovica & Forte 2004) and mineralogical data (e.g. Ivins *et al.* 1993).

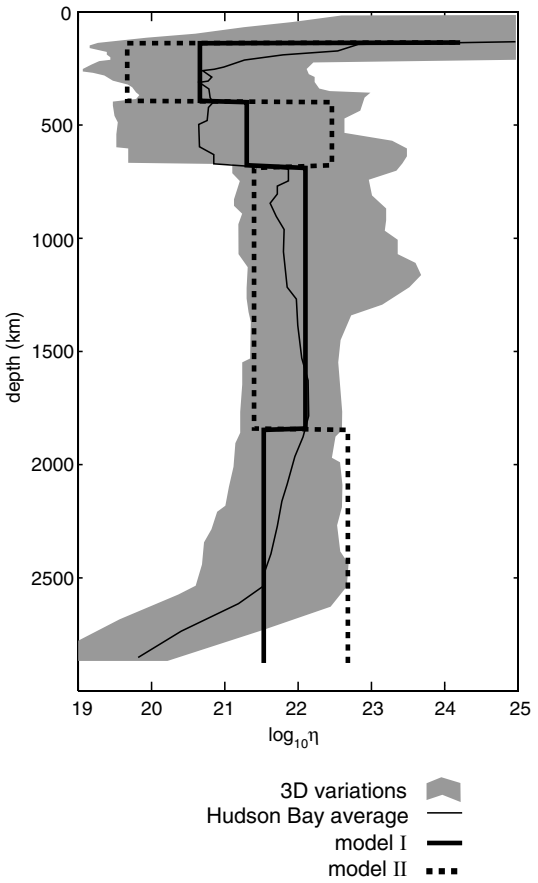

Figure 7. Models I and II from the inversion (identified in Fig. 6) are shown together with the 3-D variations (grey) and the Hudson Bay 1-D structure (thin line). While both models have a good fit to the PGR data, model I has a better recovery of the local viscosity structure. Model II exhibits the trade-off effect, where a lower viscosity in a given layer can be compensated by a higher viscosity in the neighbouring layer.

To demonstrate that the two models shown in Fig. 7 do indeed fit the synthetic PGR data, we refer to Fig. 8. Fig. 8(a) shows that RSL curves for this east coast site obtained from models I and II, although different, remain within or nearly within the errorbars. Fig. 8(b) demonstrates that both four-layer models have a nearly identical relaxation times, relative to the size of the uncertainty in these values. Fig. 8(c) shows two maps of the χ^2 values for the regional GRACE data, yielding average misfits of 1.59 and 1.73. Fig. 8(d) shows that their $\dot{J}_2$ and polar wander values are similar to each other, and are within the measurement uncertainties.

The 'trade-off' effect discussed above suggests that, while viscosities of the individual layers in the four-layer inversion are not well constrained, their whole upper- and whole lower-mantle average may be well constrained. This is also suggested by the well-constrained two-layer inversion of the previous section. To investigate this we average the upper two layers together and assign that average viscosity to the entire UM, and do the same for the lower two layers. The viscosity recovery scatter plot then becomes Fig. 6(b), where we have recomputed Δ for each of the these two-layer averages, but have not changed the χ^2 misfit. As before, the average is actually an average of the logarithms of the viscosities. Although the best viscosity recovery is now slightly larger than that of the two-layer models in Fig. 5(a), the cluster of low-misfit models do not now exhibit the highly variable values of Δ—we see the thin tail at the lowest misfits. This demonstrates that the large variability of viscosity structure observed in Fig. 6(a) was predominantly due to variations whose average remained constant, referred to above as the trade-off effect. Careful inspection shows that the thin tail of lowest misfit models in Fig. 6(b) is not as thin as that in Fig. 5(a). This is due in part to the trade-offs that may also occur between the two central layers, although these two layers are slightly de-coupled by the discontinuity between them in the true viscosity structure (at 670 km depth).

3.4 Four-layer inversion from four-layer Earth

It is natural to ask if the insensitivity of the PGR observations to viscosity trade-offs in neighbouring layers could be due to the fact that we are attempting to reproduce with a simple 1-D structure the synthetic data obtained from a much more complicated 3-D viscosity structure. To consider this we run another four-layer inversion, but this time use synthetic data generated from a four-layer 1-D model—the same four layers to be used in the forward models of the inversion. Thus we are asking: if the Earth's mantle viscosity were truly 1-D with just four layers, could an inversion from PGR data recover the correct values?

Taking the 'true' Earth viscosity shown in Fig. 7 (dotted line) and using the same uncertainties as before, we re-run the four-layer inversion. The resulting scatter plot of average viscosity difference versus PGR data misfit is shown in Fig. 9(a). As expected, there are some models that have near-zero viscosity difference to the 'true' earth structure, and produce the same PGR data as the synthetic data, yielding near-zero misfit as well. These models create the small tail which touches the origin of the plot.

Since the entire tail exists at small χ^2, however, it is misleading to consider this tail as success of the inversion. This is because the inversion has not considered the effects of noise in the synthetic data. To demonstrate this, in Fig. 9(b) we show the data from Fig. 9(a) when random noise (within the observational uncertainties) is added to the synthetic data and the misfits are recalculated. Now it is clear that taking the single model of lowest misfit will not return the correct viscosity structure.

Consideration of all models in Fig. 9(a) that fit the PGR to within uncertainties (roughly those points where $\chi^2 \leq 1$) still shows a wide variation in viscosity structures. Two points with misfits near 0.5 are labelled 'III' and 'IV' in the figure: one with high and one with low average viscosity difference to the 'true' model. Viscosity models III and IV are shown in Fig. 10. Again the trade-off effect is apparent, as model III closely follows the 'true' viscosities (shown in black) and model IV alternates about them while maintaining apparently constant averages for the entirety of the UM and LM.

To demonstrate that these two significantly different models are both reproducing the PGR data, we show these data in Fig. 11. In this figure the synthetic data are now different from those of Figs 4 and 8, since it is generated by a four-layer model rather than the full 3-D viscosity model. Though the PGR results for models III and IV are different from each other, they remain generally within the errorbars.

Thus even if the true viscosity of the Earth were as simple as a 1-D four-layer model, an inversion for this structure would still fail since the PGR data from four-layer models are insensitive to viscosity trade-offs between neighbouring layers. Although the inversion produces a single ideal model (at $\Delta = 0$ and $\chi^2 = 0$), an inversion from real data would include noise which would make all models of about $\chi^2 \leq 1$ indistinguishable. The difficulties in

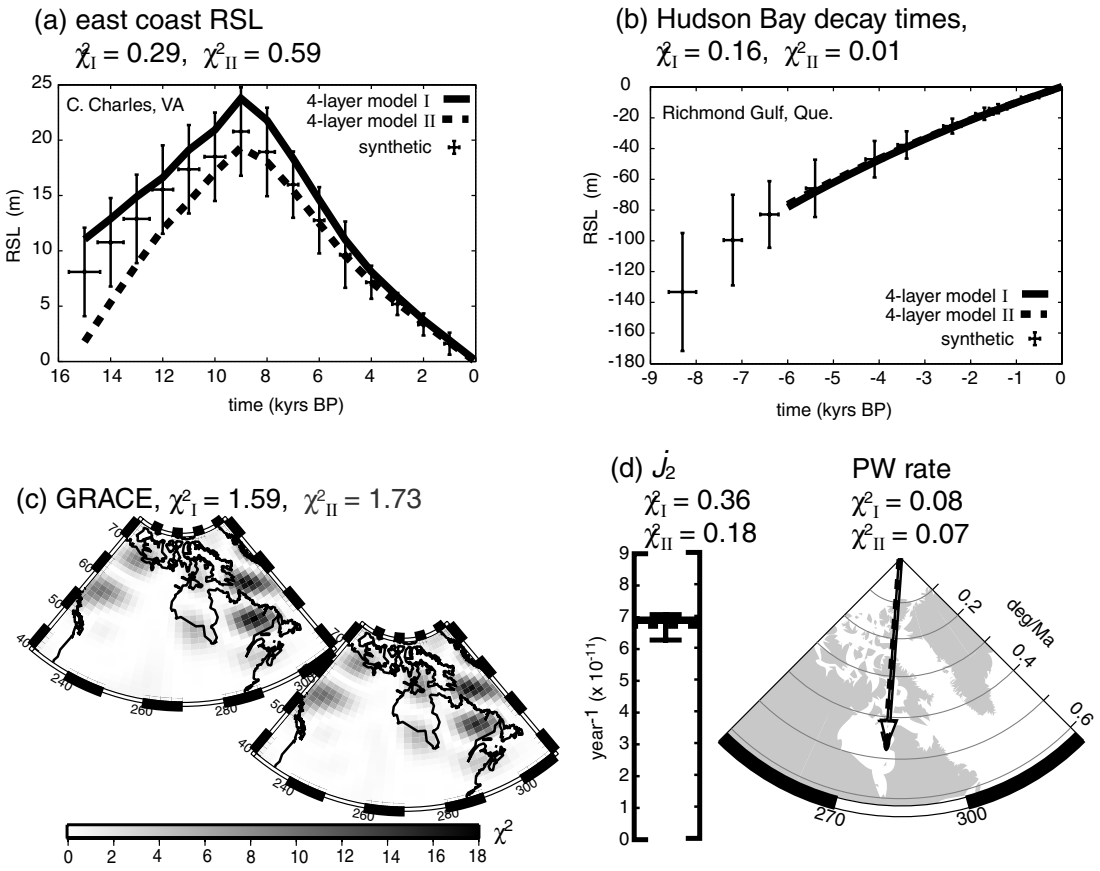

Figure 8. Demonstration that models I and II (from Figs 6 and 7) fit the PGR data about equally well. χ^2 misfit values are shown for the same PGR observations as in Fig. 4.

inverting for a realistic viscosity structure (Fig. 6a) are, therefore, not due to under-parametrization of the forward runs or to 3-D effects, but rather to the poor constraining power of the PGR observations themselves.

3.5 A resolution test

We take another look at this trade-off effect in a manner that yields a measure of the vertical resolution power of the PGR data. We perform a 20-layer inversion with the synthetic PGR data generated by a model with homogeneous mantle viscosity and elastic lithosphere. The aim is to find the vertical length scale over which these trade-offs may occur, which may be considered as the resolving power of such an inversion.

Fig. 12(a) illustrates the model that generates the synthetic data (the dashed line at 10^{21} Pa s), and an example of a 20-layer model used in the inversion. The method of inversion is as before, where all layers are allowed to vary randomly and independently until the sampling algorithm (simulated annealing augmented by the neighbourhood algorithm) begins to focus more closely on those models of low χ^2 misfit. We use the identical set of PGR data as in all previous sections. Since the model that generates the synthetic data is itself a member of the parameter space being searched (i.e. all 20 layers at 10^{21} Pa s), the inversion eventually finds this model with zero misfit. However it is the ensemble of models with $\chi^2 \leq 1$ that is of present interest.

To convert the inversion results to a measure of vertical resolution, we proceed as follows, using only those models for which $\chi^2 \leq 1$. Choose any starting layer n, where $1 \leq n \leq 20$. Among these models, the average of $\log_{10} \eta_n$ (where η_n is the viscosity in Pa s of layer n) will tend to be close to 21.0; the spread in the values of $\log_{10} \eta_n$ is defined to be one-half of its maximum minus minimum values, and labeled $s_n(1)$. Thus the nth layer of all models will tend to have $\log_{10}$-viscosities in the range $21 \pm s_n(1)$. The values of the $s_n(1)$ tend to be large—generally greater than 0.5, which indicates a viscosity uncertainty of one order of magnitude. Next, average together the values $\log_{10} \eta_n$ and $\log_{10} \eta_{n+1}$ for each model, and then average all models together to obtain viscosities in the range of $21.0 \pm s_n(2)$, where (2) represents the number of neighbouring layers averaged together. Proceeding in this way, the series $s_n(z)$ is constructed where z is the number of layers averaged together, and where the layer n is at the centre of those averaged layers (to the degree it is possible to be at the centre).

Results of this procedure are shown in Fig. 12(b), which shows the series s_n for layers $n = 3$ (centred at 380 km depth) and $n = 17$ (centred at 2260 km depth). In the figure, z, the number of layers averaged together, is replaced by the total thickness of the region averaged together; it is shown on the horizontal axis. For both s_3 and s_{17}, the greater the thickness of the region we average over, the more tightly constrained are the viscosities among the models that reasonably fit the PGR data (i.e. the values s_n are decreasing). We also see that s_3, with the shallower averaging centre, levels off more rapidly than s_{17}, at the deeper averaging centre. This suggests that the viscosity trade-offs which are responsible for the large spread in viscosities (among models that fit the PGR data) occur over shorter distances in the UM ($n = 3$) than they do in the LM ($n = 17$).

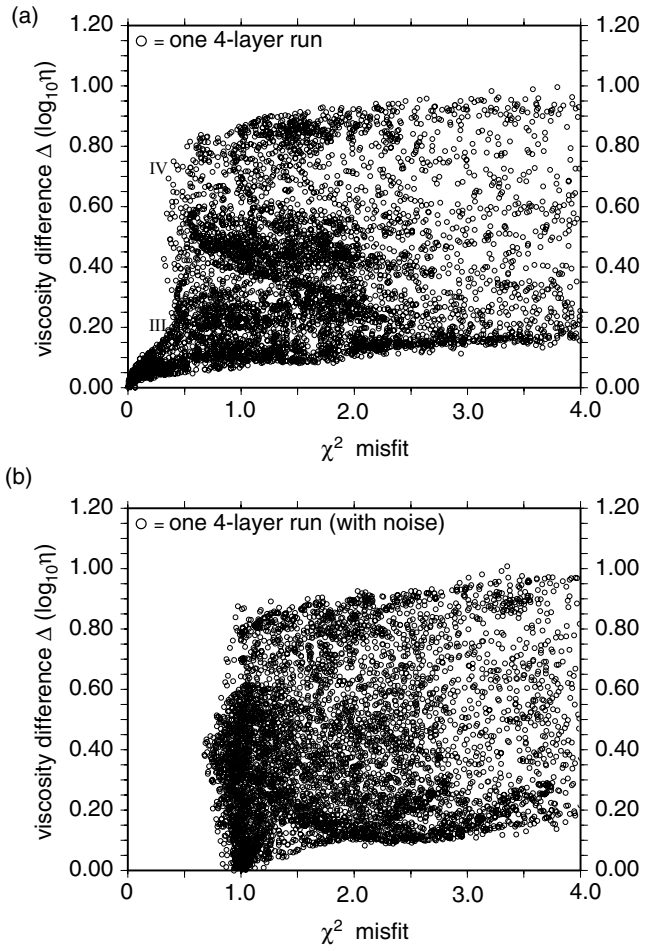

Figure 9. (a) Results of the four-layer inversion when the synthetic data are generated by a 1-D, four-layer Earth. Although there is a tail in the lower left corner of well-constrained viscosity, considering the ensemble of *all* well-fit models ($\chi^2 \leq 1$) yields a large variability in acceptable viscosities. As before, two models of low misfit (III and IV) are marked in the plot, the former with good viscosity recovery and the latter with poor viscosity recovery. (b) The misfits from Fig. 9(a) are recalculated, now with random noise in the synthetic data. Now it is clear that there remains a large ambiguity in those models of $\chi^2 \leq 1$. With some noise those models become indistinguishable.

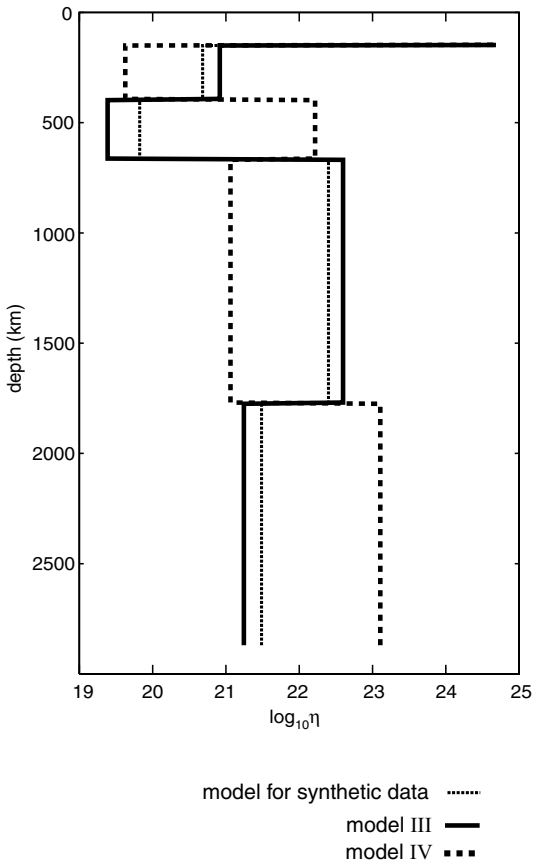

Figure 10. Models III and IV from the inversion (identified in Fig. 9) are shown together with the four-layer model that generated the synthetic data. Both models have a good fit to the PGR data, but model IV is able to do so without having a viscosity structure similar to the structure that generated the PGR data. The reason is a viscosity trade-off in neighbouring layers.

To compile the results further, we pick a value of s_n that represents a threshold: below this value we consider the average to have a spread small enough to represent a well-constrained inversion. We may then identify the averaging length required to drop below this threshold as an estimate of the length scale over which these trade-offs may occur. In this sense, we are estimating the resolving power of the inversion at various depths. Choosing a value of $s_n = 0.25$ (units of $\log_{10}$ Pa s) as such a limit, the resolution lengths at various depths are computed and shown as vertical bars in Fig. 13. (Other threshold values could be chosen, but the results would exhibit the same depth-dependence.) Also shown in the figure are the 3-D viscosity variations strictly as a visual guide. The resolution length increases with depth and has the best resolution in the UM, although the length there is about the size of the UM itself. This agrees with the observations of the previous section: although a single viscosity value for the entire UM is well-constrained in the inversion, dividing it into two layers allows it to exhibit the trade-off problems apparent in Fig. 7.

Although the resolution length in the LM is less than the height of that layer, it is not short enough to accommodate two well-constrained layers in the LM. So we are left with only two viscosity values, which may correspond to those of the entire upper and lower mantle, for which we may invert without suffering from the trade-offs in neighbouring layers. Fig. 13 may suggest that three layers of viscosity could be well-constrained, but it should be noted that this is truly only a test of the vertical resolution with respect to the 'trade-off' effect—it is highly idealized in the sense that the mantle is considered to be of homogeneous viscosity, and thus any further complications (such as a more complicated 'true' viscosity structure) would confound an inversion for three layers (such a three-layer inversion is mentioned briefly in the next section).

4 DISCUSSION AND CONCLUSION

In a search for the greatest amount of information about mantle viscosity that may be extracted from an inversion based on PGR data, we find that only two viscosity layers can be well-constrained. Since we have a natural boundary at 670 km depth, these layers may be taken to be the entire UM and the entire LM.

The PGR data are taken from a synthetic 3-D viscosity model derived from shear wave seismic tomography models. We consider RSL history for several sites along the North American east

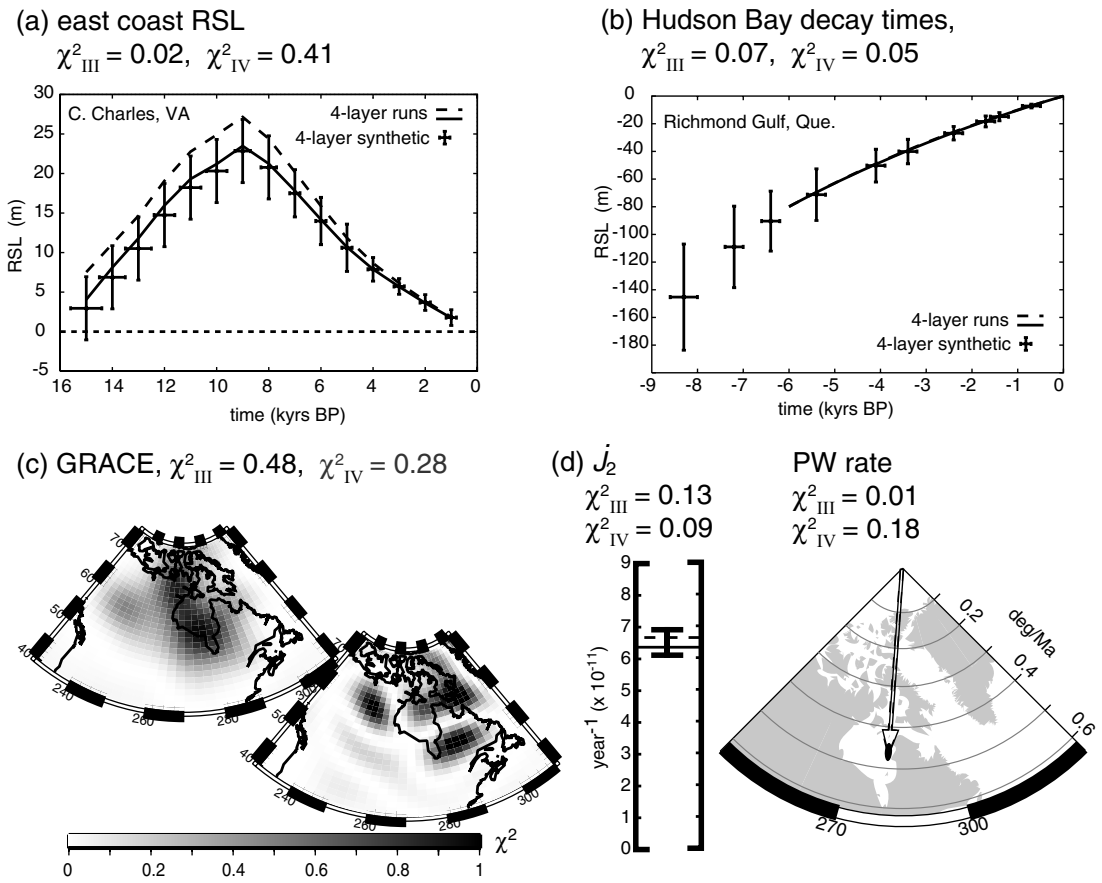

Figure 11. Demonstration that models III and IV (from Figs 9 and 10) fit the PGR about equally well. χ^2 misfit values are shown for the same PGR observations as in Fig. 4.

coast, exponential relaxation time of RSL for several sites around Hudson Bay, $\dot{J}_2$, polar wander rate, and anticipated GRACE data. We attach errorbars to these data from uncertainty values taken from published measurements so that we may consider the ensemble of all models that produce PGR data within the measurement uncertainty. Although the uncertainties on $\dot{J}_2$ and polar wander rate may be optimistically small (because we assume that the PGR contribution to these measurements is known precisely), we find that the PGR data remain unable to constrain multiple viscosity layers within the upper and LMs.

Although no two-layer model can fit all the PGR data within uncertainties, the models which fit the synthetic data best are those with viscosities corresponding to the two-layer average of the logarithm of the 3-D viscosity in the vicinity of Hudson Bay. Furthermore, all models with the smallest misfit to the PGR data have similar viscosity structures. We conclude from this that the inversion produces well-constrained values for the two viscosity layers. These findings remain true even when the inversion uses the incorrect deglaciation model, with differences similar to those between ICE-3G and ICE-4G.

Further dividing these two layers introduces degrees of freedom which the PGR data are unable to constrain. This manifests itself in a trade-off effect, in which neighbouring layers can vary greatly in viscosity provided their log-average is approximately constant. Thus, in an inversion for four layers of viscosity we find that models which maintain the correct average UM and average lower-mantle values can nevertheless vary greatly in their individual-layer viscosities. These large variations in viscosity models do not greatly affect the misfit to the PGR phenomena that we consider, at least not to an extent greater than the data uncertainties, and therefore, we cannot discriminate between them for purposes of inversion. The fact that it is the effect of viscosity trade-offs which confounds the inversion is demonstrated by the observation that when the upper two layers are (log-) averaged together, the result is well-constrained; the same is true for averaging the bottom two layers.

The trade-off effect persists even when the synthetic data, which the inversion attempts to reproduce, are generated by an earth model that itself is 1-D and has only four viscosity layers. We conclude that the trade-offs are due to the fact that the PGR data are simply insensitive to such a viscosity adjustment. Although it is natural to assume that an inversion for 1-D structure may be complicated by the true 3-D nature of the Earth's viscosity, it appears that the insensitivity of PGR to viscosity trade-offs in neighbouring layers may offer an even greater difficulty to the inversion.

We also attempt an inversion for three viscosity layers, in which either the UM or LM was divided in two. Although the results are not shown here, they simply repeat the conclusions stated above: dividing one of the initial two layers further will allow for viscosity trade-offs between the two divisions, preventing a well-constrained viscosity in the finer-resolution model.

Finally, in a more general test of the extent of the insensitivity to viscosity trade-offs, we perform a 20-layer inversion using synthetic

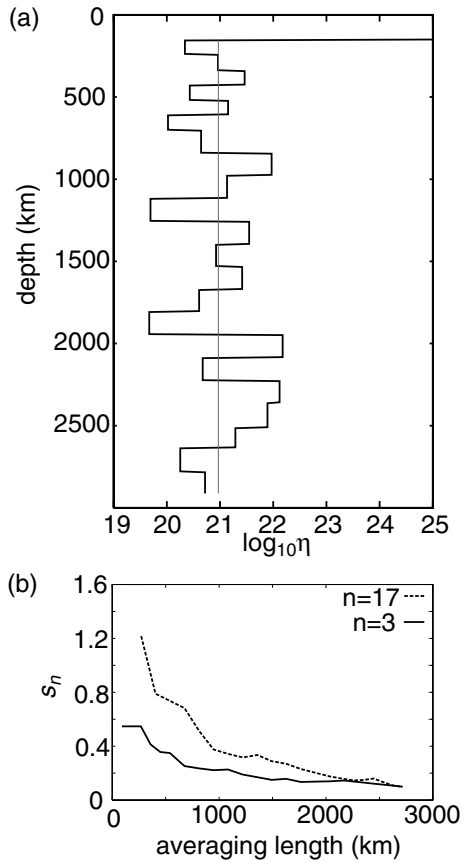

Figure 12. (a) A model from the 20-layer inversion shown as an example along side the homogeneous viscosity structure (at 10^{21} Pa s) which generates the synthetic data for this inversion. (b) The reduction in the spread of a viscosity average (s_n), as the average is taken over greater depth intervals. When the average is taken about a shallow centre ($n = 3$, solid line), the spread is smaller, indicating a shorter distance over which viscosity trade-offs may occur. A deeper averaging centre ($n = 17$, dashed line) requires a greater averaging length before the average log-viscosity converges to 21.

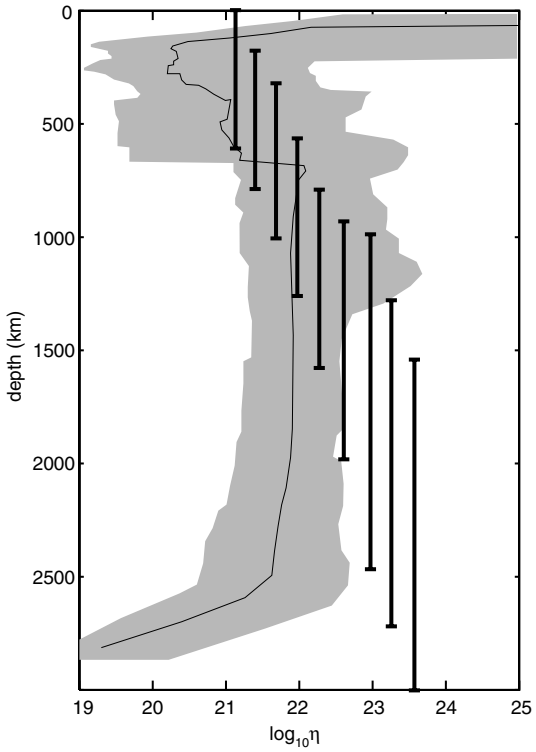

Figure 13. The averaging lengths (vertical bars) required for the spread in viscosity averages, s_n, to fall below the cut-off of 0.25. The bars are offset in the horizontal direction to make them easier to identify; there is no significance in their horizontal coordinates. The size of a bar is a rough measure of the resolution length of the inversion for the depth at which it is displayed, since it reflects the distance over which viscosity trade-offs may occur. The bars in the UM are about the size of the entire UM, and the bars in the LM are about the size of the LM. This indicates that an inversion for viscosity from PGR data can only provide two layers.

data from an Earth of homogeneous viscosity. By averaging the neighbouring layers together, we find that averages over a sufficiently thick region begin to produce well-constrained results. The thickness of that region can be considered a measure of the scale of resolution of the inversion, since over shorter distances layers may exchange viscosity without significantly altering the resulting PGR data. The size of these regions are on the order of the sizes of the UM and LM.

Although we have considered a number of PGR observables, we have not included horizontal motions. It therefore remains possible, due to the distinct constraints that such data may provide (as seen in, for example, Milne *et al.* 2004), that horizontal motions may offer hope for an improved inference of mantle viscosity structure.

ACKNOWLEDGMENTS

This research is supported by NSF grants EAR-0087567 and EAR-0134939, and by a grant from the David and Lucile Packard Foundation. We thank R. Peltier for providing the ICE-4G deglaciation model. We would also like to thank the reviewers E. Ivins and P. Wu for their thoughtful and helpful comments.

REFERENCES

Agostinetti, N.P., Spada, G. & Ciannetti, S., 2004. Mantle viscosity inference: a comparison between simulated annealing and neighbourhood algorithm inversion methods, *Geophys. J. Int.,* **157,** 890–900.

Cathles, L.M., 1975. *The Viscosity of the Earth's Mantle,* Princeton University Press, Princeton.

Cheng, M. & Tapley, B.D., 2004. Variations in the earth's oblateness during the past 28 years, *J. geophys. Res.,* **109**(B9), B09402.

Cox, C.M. & Chao, B.F., 2002. Detection of large-scale mass redistribution in the terrestrial system since 1998, *Science,* **297,** 831–833.

Farrell, W.E. & Clark, J.A., 1976. On postglacial sea level, *Geophys. J. R. astr. Soc.,* **46,** 647–667.

Forte, A.M. & Mitrovica, J.X., 1996. New inferences of mantle viscosity from joint inversion of long-wavelength mantle convection and post-glacial rebound data, *Geophys. Res. Lett.,* **23**(10), 1147–1150.

Hager, B.H., 1984. Subducted slabs and the geoid—constraints on mantle rheology and flow, *J. geophys. Res.,* **89**(B7), 6003–6015.

Hager, B.H. & Richards, M.A., 1989. Long-wavelength variations in Earth's geoid—physical models and dynamical implications, *Philos. Trans. R. Soc. London, Ser. A,* **328,** 309–327.

Ivins, E. & Sammis, C., 1995. On lateral viscosity contrast in the mantle and the rheology of low-frequency geodynamics, *Geophys. J. Int.,* **123**(2), 305–322.

Ivins, E., Sammis, C. & Yoder, C., 1993. Deep mantle viscous structure with prior estimate and satellite constraint, *J. geophys. Res.,* **98**(B3), 4579–4609.

Karato, S., 1993. Importance of anelasticity in the interpretation of seismic tomography, *Geophys. Res. Lett.,* **20,** 1623–1626.

Kaufmann, G. & Lambeck, K., 2002. Glacial isostatic adjustment and the radial viscosity profile from inverse modeling, *J. geophys. Res.,* **107**(B11), 2280.

Kaufmann, G. & Wu, P., 2002. Glacial isostatic adjustment in fennoscandia with a three-dimensional viscosity structure as an inverse problem, *Earth planet. Sci. Lett.,* **197**(1), 1–10.

Kaufmann, G., Wu, P. & Ivins, E.R., 2005. Lateral viscosity variations beneath Antarctica and their implications on regional rebound motions and seismotectonics, *J. Geodyn.,* **39**(2), 165–181.

Lambeck, K., 1995. Late Devensian and Holocene shorelines of the British-isles and North-sea from models of glacio-hydro-isostatic rebound, *J. Geol. Soc.,* **152**(3), 437–448.

Latychev, K., Mitrovica, J.X., Tromp, J., Tamisiea, M.E., Komatitsch, D. & Christara, C.C., 2005. Glacial isostatic adjustment on 3-d earth models: a finite-volume formulation, *Geophys. J. Int.,* **161,** 421–444.

Martinec, Z., Cadek, O. & Fleitout, L., 2001. Can the 1D viscosity profiles inferred from postglacial rebound data be affected by lateral viscosity variations in the tectosphere?, *Geophys. Res. Lett.,* **23,** 4403–4406.

McCarthy, D.D. & Luzum, B.J., 1996. Path of the mean rotational pole from 1899 to 1994, *Geophys. J. Int.,* **125,** 623–629.

McNamara, A.K., van Keken, P.E. & Karato, S., 2003. Development of finite strain in the convecting lower mantle and its implications for seismic anisotropy, *J. geophys. Res.,* **108**(‘B5), 2230.

Milne, G.A., Mitrovica, J.X., Scherneck, H.G., Davis, J.L., Johansson, J.M. & Vermeer, M., 2004. Continuous GPS measurements of postglacial adjustment in Fennoscandia: 2. modeling results, *J. geophys. Res.,* **109**(B2), B02412.

Mitrovica, J.X., 1996. Haskell [1935] revisited, *J. geophys. Res.,* **101**(B1), 555–570.

Mitrovica, J.X. & Forte, A.M., 2004. A new inference of mantle viscosity based upon joint inversion of convection and glacial isostatic adjustment data, *Earth planet. Sci. Lett.,* **225,** 177–189.

Mitrovica, J.X. & Peltier, W.R., 1992. A comparision of methods for the inversion of viscoelastic relaxation spectra, *Geophys. J. Int.,* **108,** 410–414.

Mitrovica, J.X. & Peltier, W.R., 1995. Constraints on mantle viscosity based upon the inversion of post-glacial uplift data from the Hudson Bay region, *Geophys. J. Int.,* **122,** 353–377.

Mitrovica, J.X., Wahr, J., Matsuyama, I. & Paulson, A., 2005. The rotational stability of an ice age earth, *Geophys. J. Int.,* **161**(2), 491–506.

Paulson, A., Zhong, S. & Wahr, J., 2005. Modelling post-glacial rebound with lateral viscosity variations, *Geophys. J. Int.,* **163**(1), 357–371.

Peltier, W.R., 1976. Glacial isostatic adjustment II. the inverse problem, *Geophys. J. R. astr. Soc.,* **46,** 669–705.

Peltier, W.R., 1994. Ice age paleotopography, *Science,* **265,** 195–201.

Peltier, W.R., 1998. Postglacial variations in the level of the sea: Implications for climate dynamics and solid-earth geophysics, *Rev. Geophys.,* **36,** 603–689.

Peltier, W.R. & Jiang, X., 1996. Mantle viscosity from the simulateous inversion of multiple data sets pertaining to postglacial rebound, *Geophys. Res. Lett.,* **23**(5), 503–506.

Richards, M.A. & Hager, B.H., 1984. Geoid anomalies in a dynamic Earth, *J. geophys. Res.,* **89**(B7), 5987–6002.

Ritsema, J., van Heijst, J.H. & Woodhouse, J.H., 1999. Complex shear wave velocity structure imaged beneath Africa and Iceland, *Science,* **286,** 1925–1928.

Sambridge, M., 1999. Geophysical inversion with a neighborhood algorithm–I. searching a parameter space, *Geophys. J. Int.,* **138,** 479–494.

Shapiro, N. & Ritzwoller, M., 2004. Thermodynamic constraints on seismic inversions, *Geophys. J. Int.,* **157**(3), 1175–1188.

Simons, M. & Hager, B.H., 1997. Localization of the gravity field and the signature of glacial rebound, *Nature,* **390,** 500–504.

Steffen, H. & Kaufmann, G., 2005. Glacial isostatic adjustment of Scandinavia and northwestern Europe and the radial viscosity structure of the Earth’s mantle, *Geophys. J. Int.,* **163**(2), 801–812.

Tushingham, A.M. & Peltier, W.R., 1991. ICE-3G: a new global model of late Pleistocene deglaciation based upon geophysical predictions of post-glacial relative sea level change, *J. geophys. Res.,* **70**(B3), 4497–4523.

Tushingham, A.M. & Peltier, W.R., 1992. Validation of the ICE-3G model of Wurm-Wisconsin deglaciation using a global data base of relative sea level histories, *J. geophys. Res.,* **97**(B3), 3285–3304.

van der Lee, S., 2002. High-resolution estimates of lithospheric thickness from Missouri to Massachusetts, USA, *Earth planet. Sci. Lett.,* **203**(1), 15–23.

Velicogna, I.J. & Wahr, J., 2002. Postglacial rebound and earth’s viscosity structure from GRACE, *J. geophys. Res.,* **107**(B12), 2376.

Wahr, J., Wingham, D. & Bentley, C., 2000. A method of combining icesat and grace satellite data to constrain antarctic mass balance, *J. geophys. Res.,* **105**(B7), 16279–16294.

Wahr, J., van Dam, T., Larson, K. & Francis, O., 2001. Geodetic measurements in Greenland and their implications, *J. geophys. Res.,* **106**(B8), 16 567–16 582.

Wahr, J., Swenson, S., Zlotnicki, V. & Velicogna, I., 2004. Time-variable gravity from GRACE: first results, *Geophys. Res. Lett.,* **31**(11), L11501.

Wu, P. & Peltier, W.R., 1982. Viscous gravitational relaxation, *Geophys. J. R. astr. Soc.,* **70,** 435–485.

Wu, P. & Peltier, W.R., 1984. Pleistocene deglaciation and the earth’s rotation: a new analysis, *Geophys. J. R. astr. Soc.,* **76,** 753–792.

Wu, P. & van der Wal, W., 2003. Postglacial sealevels on a spherical, self-gravitating viscoelastic earth: effects of lateral viscosity variations in the upper mantle on the inference of viscosity contrasts in the lower mantle, *Earth planet. Sci. Lett.,* **211**(1), 57–68.

Yamazaki, D. & Karato, S., 2001. Some mineral physics constraints on the rheology and geothermal structure of the earth’s lower mantle, *Am. Mineral.,* **86,** 385–391.

Zhong, S., Paulson, A. & Wahr, J., 2003. Three-dimensional finite-element modelling of Earth’s viscoelastic deformation: effects of lateral variations in lithospheric thickness, *Geophys. J. Int.,* **155**(2), 679–695.